Published in final edited form as:
Biomaterials. 2008 July ; 29(19): 2839–2848.

Physical Properties and Cellular Responses to Crosslinkable Poly (Propylene Fumarate)/Hydroxyapatite Nanocomposites

Kee-Won Lee[1], **Shanfeng Wang**[2], **Michael J. Yaszemski**[1], and **Lichun Lu**[1,*]

1*Departments of Orthopedic Surgery and Biomedical Engineering, Mayo Clinic College of Medicine, 200 First Street SW, Rochester, Minnesota 55905*

2*Department of Materials Science and Engineering, The University of Tennessee, Knoxville, Tennessee 37996*

Abstract

A series of crosslinkable nanocomposites has been developed using hydroxyapatite (HA) nanoparticles and poly(propylene fumarate) (PPF). PPF/HA nanocomposites with four different weight fractions of HA nanoparticles have been characterized in terms of thermal and mechanical properties. To assess surface chemistry of crosslinked PPF/HA nanocomposites, their hydrophilicity and capability of adsorbing proteins have been determined using static contact angle measurement and MicroBCA protein assay kit after incubation with 10% fetal bovine serum (FBS), respectively. *In vitro* cell studies have been performed using MC3T3-E1 mouse pre-osteoblast cells to investigate the ability of PPF/HA nanocomposites to support cell attachment, spreading, and proliferation after 1, 4, and 7 days. By adding HA nanoparticles to PPF, the mechanical properties of crosslinked PPF/HA nanocomposites have not been increased due to the initially high modulus of crosslinked PPF. However, hydrophilicity and serum protein adsorption on the surface of nanocomposites have been significantly increased, resulting in enhanced cell attachment, spreading, and proliferation after 4 days of cell seeding. These results indicate that crosslinkable PPF/HA nanocomposites are useful for hard tissue replacement because of excellent mechanical strength and osteoconductivity.

Keywords

Poly(propylene fumarate) (PPF); Hydroxyapatite (HA); Nanocomposite; Protein adsorption; Osteoblast response

1. Introduction

Calcium phosphate ceramic materials have been used for skeletal tissue engineering applications because of their excellent biocompatibility and osteoconductive properties [1,2]. Among these materials, hydroxyapatite [HA, $Ca_{10}(PO_4)_6(OH)_2$] is the major inorganic compound and has similar chemical and crystal structure to bone mineral. Thus HA has been studied extensively as an excellent osteoconductive material. However, it is very brittle and cannot be applied to the load-bearing site directly [3-5].

*Corresponding author: Lichun Lu, Ph.D., Associate Professor of Orthopedics and Biomedical Engineering, Mayo Clinic College of Medicine, 200 First Street SW, MS 3-69, Rochester, MN 55905, Phone: 507-538-4987, Fax: 507-284-5075, E-mail: lu.lichun@mayo.edu.

To overcome these limitations, HA has been incorporated with natural biomacromolecules such as collagen [6-8] and gelatin [9,10], or synthetic polymers such as poly (α-hydroxyl acids) [11-15], poly (ε-caprolactone) (PCL) [16,17], polyamide [18], and polymethylmethacrylate (PMMA) [19] to prepare composites using a variety of methods including surface coating, grafting, direct mixing, and biomimetic precipitation [10,11,20-23]. Particularly, polymer/HA nanocomposites have improved mechanical properties and enhanced cell attachment, spreading, and proliferation on their surfaces by adding nano-sized HA to modify the polymer's characteristics and/or strengthen the polymer matrix [24,25]. Oftentimes, these nanocomposites still cannot achieve the targeted compressive strength and modulus for load-bearing applications because the matrix polymers themselves do not have sufficient mechanical properties to be improved upon.

One of the promising candidate materials with suitable mechanical properties for load-bearing applications is poly(propylene fumarate) (PPF). It is an unsaturated linear polyester that can be crosslinked through carbon-carbon double bonds along its backbone [26,27] and degraded through simple hydrolysis of the ester bonds into non-toxic products of propylene glycol, poly (acrylic acid-*co*-fumaric acid), and fumaric acid [28]. By controlling the molecular weight of PPF and the crosslinking density, the maximum compressive strength and modulus of crosslinked PPF can be over 10 and 100 MPa, respectively [29-32]. Although many previous studies have been performed to enhance both mechanical strength and osteoconductive properties by adding calcium phosphate such as β-tricalcium phosphate (β-TCP) to PPF [33, 34], or preparing PPF/HA composites by either simple mixing [35] or from *in situ* precipitation [36], the correlation between the physical properties and cell responses on PPF/HA nanocomposites has not yet been reported, compared with other poly(α-hydroxyl acids)-based composites.

As a prelude to a further study on three dimensional (3D) PPF/HA nanocomposite scaffolds with different features fabricated using solid freeform technique [37], we report a series of crosslinkable nanocomposites based on PPF and HA nanoparticles and their two dimensional (2D) disks prepared through thermal crosslinking. In this report, we will reveal the role of HA nanoparticles in modifying the surface properties and controlling *in vitro* cell responses. The structure, morphology, and physical properties of the crosslinked PPF/HA nanocomposites have been characterized using Fourier transform infrared (FTIR) spectroscopy, wide-angle X-ray diffraction (WAXD), thermogravimetric analysis (TGA), transmission electron microscopy (TEM), scanning electron microscopy (SEM), atomic force microscopy (AFM), and dynamic mechanical analyzer (DMA). In addition, hydrophilicity and the capability of adsorbing serum proteins on the crosslinked PPF/HA disks have been determined from static contact angle measurement and MicroBCA protein assay kit, respectively. To investigate *in vitro* cellular responses, MC3T3-E1 cells were seeded and cultured on the PPF/HA nanocomposite disks. Cell morphology after 24 h was imaged using SEM. Cell spreading was examined by F-actin staining with rhodamine-phalloidin and cell proliferation was quantified using a colorimetric MTS assay at 1, 4, and 7 days.

2. Materials and methods

2.1. PPF synthesis

As described previously [31,32], diethyl fumarate (DEF) and excess amount of 1,2-propylene glycol were polymerized together with hydroquinone (crosslinking inhibitor) and zinc chloride (catalyst) first at 100 °C for 1 h and then 150 °C for 7 h to obtain the intermediate dimer. Then the intermediate dimer was transesterified to form PPF under vacuum at 130 °C for another 4 h. Gel permeation chromatography (GPC) was used to determine the molecular weight and polydispersity of PPF. GPC was carried out with a Waters 717 Plus Autosampler GPC system (Waters, Milford, MA) connected to a model 515 HPLC pump and model 2410 refractive index

detector. Mono-dispersed polystyrene standards (Polysciences, Warrington, PA) with peak molecular weights (M_p) of 474, 6690, and 18600 g.mol^{-1} were used to construct the calibration curve. The M_n and weight average molecular weight (M_w) of the synthesized PPF were 3460 and 7910 g.mol^{-1}, respectively. The chemical structure of PPF is shown in Scheme 1.

2.2. PPF/HA nanocomposite preparation

HA nanoparticles were purchased from Berkeley Advanced Biomaterials (Berkeley, CA). The size range of HA nanoparticles is from 20 to 550 nm (average size = 100 nm) and their whiskers have long and short axis of ~100 and ~20 nm, respectively. PPF and HA were crosslinked by a free radical polymerization using 1-vinyl-2-pyrrolidinone (NVP), benzoyl peroxide (BPO) and *N*-dimethyl-*p*-toluidine (DMT) as crosslinker, free radical initiator, and accelerator, respectively. One gram of PPF and 0.4 g of NVP, corresponding to 40% NVP per gram of PPF, were mixed in a glass vial at 37 °C for 2 h. Then, four different amounts of HA were added into PPF solutions to prepare PPF/HA mixtures with HA weight fractions of 0, 10, 20, and 30%. Forty microliters of initiator solution (50 mg of BPO in 250 μL of NVP) and 16 μL of accelerator solution (20 μL of DMT in 980 μL of methylene chloride) were added and mixed thoroughly. Compositions of PPF/HA mixtures are listed in Table 1. The resulting PPF/HA mixtures were poured into cylindrical glass molds with a diameter of 10 mm and a height of 30 mm. The loaded molds were placed in a convection oven at 60 °C for 1 h to facilitate crosslinking. After crosslinking, the molds were cooled down to room temperature. Crosslinked PPF/HA specimens were removed from the molds, and cut into disks with a diameter of 10 mm and a thickness of 1 mm using an Isomet low speed saw (Buehler, Lake Bluff, IL).

2.3. PPF/HA disk characterization

Fourier transform infrared spectroscopy (FTIR) spectra were obtained on a Nicolet 550 spectrometer (Thermo Scientific Inc., Waltham, MA). All samples were analyzed using a zinc selenide ATR crystal. The resolution of the instrument was specified as 4 cm^{-1} at a wavenumber of 1000 cm^{-1}.

Wide-angle X-ray Diffraction (WAXD) measurements were performed in the X-ray scattering lab of Characterization Facility at the University of Minnesota. The small pieces from the disks were suspended and run in transmission mode. The microdiffractometer (Bruker AXS Inc., Madison, WI) with copper radiation, an incident beam monochromater, and a GADDS multiwire area detector were used for the wide angle tests. Two frames were collected, one at 2θ=20° and one at 50 ° to cover a range of 5 ° to 65 ° for 2θ. Each frame was collected for 5 min. The data was then integrated and plotted as intensity vs. 2θ.

Thermogravimetric analysis (TGA) was done using a thermogravimetric analyzer (Q500, TA Instruments, New Castle, DE). TGA data of the crosslinked PPF and PPF/HA nanocomposites were obtained in flowing nitrogen at a heating rate of 20 °C.min^{-1}.

Morphology of HA nanoparticles in the crosslinked PPF/HA disks was examined by a transmission electron microscope (TEM) (1200-EX II, JEOL Inc., Japan). The sample was placed into plastic capsules filled with resin, hardened into at 60 °C for 24 h, and sectioned with a glass knife as a thick block by a thickness of 0.6 μm. For TEM imaging, the block was trimmed down to the area of interest and then sectioned with a diamond knife by a thickness of 0.1 μm. All samples were viewed at 80 kV accelerating voltage.

Surface morphology of the crosslinked PPF and PPF/HA disks was examined by a cold-field emission scanning electron microscope (SEM) (S-4700, Hitachi Instruments Inc., Japan). For

SEM imaging, the sample was mounted onto an aluminum stub, sputter coated with gold-palladium, and viewed at 3 kV accelerating voltage.

Atomic force microscopy was performed on a Nanoscope III multimode AFM (Veeco Instruments, CA). Topography of the surface (height image) was captured in contact mode imaging with 50×50 μm^2 scan size. Si3N4 tip with nominal spring constant of 0.58N/m and tip size (radius of curvature) of ~10 nm was used for all scans. The height images were flattened with 1st order polynomial function to remove the background and the Root mean square (RMS) roughness was calculated from processed images.

Compression testing for the crosslinked PPF and PPF/HA disks was implemented by dynamic mechanical analyzer (DMA 2980, TA instruments). Before testing, initial cross-sectional area and dimension of each sample were measured. All samples were compressed at a rate of 1 $mm.min^{-1}$. Compressive modulus was calculated from the slope of the linear region in the stress-strain curve.

A static contact angle measurement system was used to determine the hydrophilicity of the crosslinked PPF and PPF/HA disks. Approximately 1 μL of water (pH=7.0) was dropped on the disk surface. Contact angle measurement was made after a static time of 30 sec. A tangent method was used to calculate the contact angle in degrees. For each composition, three disks were used and six data points were taken for mean and standard deviation calculation.

Pre-wetted disks in phosphate-buffered saline (PBS) (Cellgro, Mediatech Inc., Herndon, VA) for 24 h were put into the culture media supplemented with 10% fetal bovine serum (FBS) (Gibco, Invitrogen Corp., Carlsbad, CA) for 4 h at 37 °C. Then these disks were transferred into 48-well plates (one disk per well) and washed with 600 μL PBS three times. Five minutes' gentle agitation was applied and PBS was discarded after each wash. Two hundred forty microliters of 1% sodium dodecyl sulfate (SDS) solution was added into those wells and left for 1 h for detaching proteins from the disk surfaces. This procedure was repeated twice and all the SDS solution with detached protein was collected in a plastic vial. Protein concentration in the collected SDS solutions was determined from a microplate reader (SpectraMax Plus 384, Molecular Devices, Sunnyvale, CA) using a MicroBCA Protein assay kit (Pierce, Rockford, IL). Albumin in the kit was used to prepare solutions in SDS with eight known concentrations to construct a standard curve.

2.4. Cell culture

MC3T3-E1 mouse pre-osteoblast cells were cultured *in vitro* using Dulbecco's modified Eagle's medium (DMEM) F-12 (Sigma-Aldrich, St. Louis, MO), supplemented with 10% FBS and 1% penicillin/streptomycin (Gibco). Crosslinked PPF/HA disks were sterilized in 70% ethanol for 24 h, washed in PBS (pH=7.4) three times, and then pre-wetted by immersing them in culture media for 24 h before cell seeding. Cells were seeded on pre-wetted disks at a density of 20,000 $cells.cm^{-2}$ and cultured for 1, 4, and 7 days in a humidified atmosphere of 5% CO_2 at 37 °C.

2.5. Cell attachment and morphology

Cell morphology on the crosslinked PPF and PPF/HA disks was examined using SEM after 24 h of cell seeding. Culture media was removed from the disks and the cells were fixed with Trump solution composed of 4% formaldehyde and 1% glutaraldehyde in PBS. After removing the fixative, the disks were subsequently washed in PBS and distilled water. For SEM imaging, the disks were dehydrated through a graded series of ethanol (60, 70, 80, 95, and 100%), critical point dried, mounted onto an aluminum stub, and then sputter-coated with gold-palladium. All samples were viewed at 3 kV accelerating voltage.

2.6. Cell spreading and proliferation

Cell spreading was examined by F-actin staining with rhodamine-phalloidin (Molecular Probes, Eugene, OR) at three different time points (1, 4, and 7 days). After removing the culture media, the disks were rinsed with PBS twice and cells were fixed with 2% paraformaldehyde for 20 min and 0.2% Triton X-100 for 2 min at room temperature sequentially, with PBS rinsing for three times between these two steps. F-actin staining was performed by removing PBS from the disks, adding 200 μL of reagent solution (80 μL of rhodamine-phalloidin in 12 mL of PBS) in each well and incubating them for 1 h. All images were viewed and captured using an optical fluorescence microscope (Zeiss Axiovert 35, Carl Zeiss, Thornwood, NY) equipped with a Nikon CCD camera in a 555/565 nm (excitation/emission) filter set. Cell proliferation was quantified using a colorimetric CellTiter96® AQueous One Solution (MTS) Assay (Promega, Madison, WI) at 1, 4, and 7 days following the manufacturer's instruction. The number of living cells in each sample was correlated to the UV absorbance at 490 nm measured using a microplate reader.

2.7. Statistical analysis

All measured data were reported as means±standard deviations for $n = 5$, except for the AFM study where two scan areas from three different samples were analyzed for each PPF and PPF/HA group. One-way analysis of variance (ANOVA) and Tukey-Kramer post-hoc test were performed using StatView software (SAS Institute, Cary, NC) to assess the statistical difference at a significance level of $p<0.05$.

3. Results and Discussion

3.1. Structural characterizations and morphology

The chemical structure of crosslinked PPF and its composites with HA were characterized by FTIR spectra as shown in Figure 1. The FTIR spectra (not shown here) for uncrosslinked PPF and pristine HA nanoparticles have strong absorption peaks at 3440 cm^{-1} to indicate hydroxyl groups; however, these peaks are not prominent in the crosslinked PPF and PPF/HA nanocomposites. The absorption peaks are similar in all the FTIR spectra with a significant increase in the intensity of the absorption peak at 1000 cm^{-1} as the composition of HA increases because this absorption peak is due to the phosphate group in HA [17]. The absorption peaks assigned to methylene ($-CH_2-$) and ester carbonyl (-C=O) groups are present at 2950 and 1740 cm^{-1}, respectively.

The WAXD patterns of crosslinked PPF and PPF/HA nanocomposites with different HA compositions are shown in Figure 2. PPF is an amorphous polymer with a glass transition temperature (T_g) varying with molecular weight up to 31.9 °C at infinite-molecular-weight [27]. Crosslinked PPF disks are also amorphous and transparent, demonstrated by a broad diffraction peak centered at a 2θ value of 20° in Figure 2. In contrast, HA nanoparticles are typical crystalline structures with sharp diffraction peaks that can be assigned to different planes as marked in the pattern for PPF/HA (10%), in agreement with JCPDS files for high temperature sintered HA [38]. The diffraction peaks for HA are all present in the PPF/HA nanocomposites. The intensity of the broad peak attributing to crosslinked PPF decreases with increasing HA composition. However, unlike *in situ* formation of HA crystals in the presence of polymer or gelatin matrix [36,39], the intensities of all peaks for HA do not change significantly because simple blending of preformed HA with amorphous PPF matrix does not influence the crystalline structure of HA.

Figure 3 shows the TGA thermograms of crosslinked PPF and PPF/HA nanocomposites with three different HA compositions. In the observation temperature range up to 700 °C, HA is stable without significant weight drop (<5%) (data not shown) while crosslinked PPF has one

thermal degradation step. The onset degradation temperature T_d for crosslinked PPF is 341 °C and it increases slightly with the composition of HA. It should be noted that the residue after the degradation of crosslinked PPF increases progressively with the composition of HA. Given the weight fraction of residue for crosslinked PPF, which is 10.6%, one can predict the weight fractions of residue for the crosslinked PPF/HA nanocomposites with different HA compositions. The calculated values are 19.5%, 28.5%, and 37.4%, in satisfactory agreement with the experimental values of 19.3%, 25.5%, and 36.3% for the crosslinked PPF/HA nanocomposites with HA compositions of 10, 20, and 30%, respectively. It confirms that the compositions of the final crosslinked PPF/HA nanocomposites are consistent with the feed ratios of both components before crosslinking.

Morphology of HA nanoparticles in the crosslinked PPF/HA disks is shown in the TEM images in Figure 4. HA particles were dispersed or aggregated in the disks. TEM images at a magnification of 30,000× show niddle-like HA nanoparticles with their long and short axis of ~100 and ~20 nm, respectively. These results demonstrate that HA nanoparticles can be dispersed well in the polymer matrix by simple mixing and crosslinking with PPF, with distribution similar to previously reported surface grafting [22,23] of HA nanoparticles for polymer/HA nanocomposites.

Moreover, surface morphology of crosslinked PPF and PPF/HA disks is shown in Figure 5. Because the crosslinked PPF/HA nanocomposite disks were cut using a saw from a whole polymer cylinder, the surfaces reflect the inner structure with the possibility of having direct HA moiety instead of HA wrapped completely within PPF. Therefore the role of HA in modifying nanocomposite's properties is to serve not only as a physical filler to the polymer matrix but also an additive onto the surface to change its chemistry. SEM images in Figure 5 verify this design by showing that different sizes of white spots (HA particles) were dispersed well on the surface of disks.

To elucidate the effect of HA incorporation on the surface roughness of 2D surfaces, AFM was performed on the cut PPF and PPF/HA disks. Representative 3D renderings of the sample surfaces are shown in Figure 6A. The average root mean square (RMS) roughness of the samples ranged from 346.7±24.4 nm for PPF to 473.6±39.9 nm for PPF/HA 10% (Figure 6B). No correlation between surface roughness and HA composition was observed. All samples had similar surface roughness ($p > 0.05$) as a result of the same cutting method for 2D sample preparation.

As shown in Figure 7, the stress vs. strain curves for crosslinked PPF and PPF/HA disks are similar, resulting in only slight increase in compressive modulus with increasing HA composition. The compressive moduli range from 135±18 to 150±40 MPa without significant differences among samples. Unlike previously reported results of increased mechanical strength of crosslinked PPF composites by adding calcium phosphate such as β-TCP [33,34], in this study the addition of HA nanoparticles does not increase mechanical strength of the final crosslinked PPF/HA nanocomposites. It can be interpreted by the fact that PPF used in this study has a fairly high molecular weight to render a rigid crosslinked PPF with a compressive modulus of over 100 MPa. Considering previously reported compressive modulus (50~500 MPa) [40] of human trabecular bone, our results show that PPF/HA nanocomposites have sufficient mechanical strength for bone tissue engineering applications.

3.2. Hydrophilicity and protein adsorption

As mentioned earlier and demonstrated by SEM pictures in Figure 5, HA particles can appear on the disk surface instead of being coated by crosslinked PPF as the result of cutting preparation method. Consequently, HA will modify the surface chemistry including hydrophilicity and the capability of adsorbing protein, while maintain similar surface

roughness. Figure 8 shows photographs of water droplets and static contact angles of crosslinked PPF and PPF/HA disks. The height of droplet on the surface of disks decreases with increasing HA composition (Figure 8A). On the crosslinked PPF disks, increased size and height of droplets can be clearly observed, while on PPF/HA disks, droplets are more spread out on the surface as HA composition increases. The measured static contact angle decreases with increasing HA composition and the differences between crosslinked PPF and other PPF/HA disks are significant ($p<0.05$) (Figure 8B). On the crosslinked PPF disks, the water contact angle is 68.9±8.2°, whereas it decreases abruptly as HA composition increases. The minimum value was found on the PPF/HA disk with 30% HA at 34.9±3.7°. These results show that the incorporation of HA nanoparticles with crosslinked PPF increases the hydrophilicity on their surfaces, in agreement with previous studies on other biodegradable synthetic polymer matrixes [15,41].

The effect of HA nanoparticles to crosslinked PPF was also investigated on the capability of adsorbing protein from the media supplemented with 10% FBS. As shown in Figure 9, the total amount of adsorbed protein measured using a MicroBCA Protein assay kit is significantly greater on crosslinked PPF/HA disks than that on crosslinked PPF disks. For crosslinked PPF/HA disks, adsorbed protein only slightly increases as HA composition increases with no significant differences among different HA compositions. It has been found that serum protein adsorption can be significantly improved on a surface of nano-sized ceramic materials compared with micro-sized ceramic materials [14,40,41]. Our results demonstrate that the addition of HA nanoparticles increases serum protein adsorption significantly on the surface of PPF disks.

3.3. In vitro cell studies

Figure 10 shows SEM images of crosslinked PPF and PPF/HA disks 24 h after cell seeding. Cells attached to the surfaces of each sample displayed a flat and well-spread morphology since 24 h is sufficient for initial cell attachment onto the disk surfaces. It can be observed that more cells attached and more protruding cellular processes were developed for connection between adjacent cells on the HA-containing surfaces. The present observation is in agreement with MC3T3-E1 cell behavior on the surfaces of other polymer/HA composites [42]. Because the attachment of anchorage-dependent cells such as osteoblasts involves short-term events like physicochemical linkages between cells and materials, surface properties of materials including surface rigidity, surface roughness from topology, and surface chemistry strongly affect the quality of attachment [43]. In the present study, enhanced initial cell attachment of PPF/HA disks was largely affected by surface wettability rather than by surface topology. As aforementioned in sample preparation, since all samples were cut into disks with the same saw and the size of HA particles was very small, the effect of roughness due to exposed nano-HA particles on the surface of PPF/HA disks was insignificant, as shown by the similar surface roughness of all specimens from the AFM study (Figure 6). In contrast, hydrophilicity was significantly increased with incorporating HA into the polymer matrix. It is noted that certain hydrophilic surfaces with a contact angle of around 50° or lower (Figure 8) generally have better initial cell attachment than hydrophobic surfaces [44]. Our results provide the evidence that increased hydrophilicity by adding nano-HA particles enhances initial pre-osteoblast cell attachment on the surface of PPF/HA nanocomposites.

Increased initial cell attachment on PPF/HA surfaces as compared to PPF alone is also attributed to the increased total amount of adsorbed proteins shown in Figure 9. Proteins such as fibronectin or vitronectin have been known to promote *in vitro* cell adhesion, particularly osteoblast [43]. These features have been reported from protein adsorption measurements on the surface of other substrates or polymer/calcium phosphate nanocomposites using human serum or FBS in many previous efforts [10,14,42,47,48]. Recently, Woo et al. [49] showed

more amount of adsorbed specific serum proteins such albumin, fibronectin, and vitronectin as well as higher DNA content of MC3T3-E1 cells cultured on poly(L-lactic acid)(PLLA)/HA composite scaffolds than on PLLA scaffolds only. Our results were consistent with previous studies and demonstrate that increased protein adsorption on PPF/HA nanocomposites leads to increased initial cell attachment.

Besides initial cell attachment, cytoskeletal organization and cell spreading were examined by F-actin staining with rhodamine-phalloidin of crosslinked PPF and PPF/HA disks at three different time points as shown in Figure 11. At 1 day, cells on the surface of PPF and PPF/HA disks displayed some actin filaments, and cells were mostly isolated on crosslinked PPF while more cell-cell interactions were seen on PPF/HA (20 and 30%). After 4 days, fully connected, complex networks of actin filaments throughout attached cells were observed on PPF/HA disks as HA composition increases. This actin cytoskeleton organization is a prerequisite for maintaining cell morphology and adhesion between cultured cells and substrate surfaces and also for facilitating subsequent cell spreading and proliferation [43], and may be promoted through enhanced adsorption of extracellular matrix proteins from the culture milieu [45,46]. The present experimental data reveal that the addition of HA nanoparticles enhances cell spreading as well as cytoskeleton organization on PPF/HA nanocomposites, demonstrating increased complex actin filaments as HA composition increases.

Cell proliferation on crosslinked PPF and PPF/HA disks over a 7-day period was indirectly quantified by the MTS assay. As shown in Figure 12, cell density, which directly correlates to the MTS absorption, was significantly lower on PPF and PPF/HA (10 and 20%) disks than PPF/HA 30% and control TCPS after 1 day of culture. It is noted that at day 1, only PPF/HA 30% disks showed significant difference in cell density from PPF alone surfaces, even though both hydrophilicity and protein adsorption were significantly improved with increasing HA compositions. This finding implies that MC3T3 cell proliferation on PPF/HA disks was affected by substrate surface properties as well as intrinsic patterns of cell growth. Kennedy et al. [50] reported recently that MC3T3 cell numbers did not increase from 8 to 24 h after culture on glass self-assembled monolayer (SAM) slides with different surface energy gradients by using UV exposures, but increased at 64 and 136 h as cells proliferated. In the present study, cell density on all PPF/HA disks was significantly higher than on PPF disks after 4 days, revealing that cell proliferation increased more than 37% compared with PPF disks. These results indicate that cell proliferation was significantly enhanced by incorporation of nano-HA particles in the PPF/HA composites.

4. Conclusions

In summary, we have prepared PPF/HA nanocomposites by crosslinking HA nanoparticles and PPF. PPF/HA nanocomposites with four different weight fractions of HA nanoparticles have been characterized in terms of surface morphology, thermal and mechanical properties. TEM and SEM images showed that HA nanoparticles were dispersed well on the polymer surface with increasing HA composition. In compressive testing, HA nanoparticles did not have much effect on increasing mechanical strength due to the initially high rigidity of PPF itself. However, from static contact angle and protein adsorption measurements, we have shown that the addition of HA nanoparticles increased hydrophilicity and serum protein adsorption on the surface of nanocomposites. PPF/HA surfaces enhanced pre-osteoblast cell attachment, spreading, and proliferation after 4 days of culture. The results of present study, thus, demonstrate that crosslinkable PPF/HA nanocomposites may serve as a scaffolding material for bone tissue engineering applications needing sufficient mechanical strength as well as good osteoconductivity.

Acknowledgements

This study was funded by the Mayo Foundation and National Institutes of Health (R01 AR45871 and R01 EB003060). The authors would like to thank Mr. James A. Gruetzmacher for help with PPF synthesis and Dr. Theresa E. Hefferan for assistance with cell culture. Wide-angle X-ray diffraction and atomic force microscopy measurements were carried out in the Institute of Technology Characterization Facility, University of Minnesota, which receives partial support from NSF through the NNIN program.

References

1. Jarcho M, Kay JF, Gumar KI, Doremus RH, Drobeck HP. Tissue, cellular and subcellular events at a bone-ceramic hydroxylapatite interface. J Bioeng 1977;1:79–92. [PubMed: 355244]
2. Hollinger JO, Battistone GC. Biodegradable bone repair materials Synthetic polymers and ceramics. Clin Orthop Relat Res 1986;207:290–305. [PubMed: 3522015]
3. Lemons JE. Hydroxyapatite coatings. Clin Orthop Relat Res 1988;235:220–3. [PubMed: 3416527]
4. Burg KJL, Porter S, Kellam JF. Biomaterial developments for bone tissue engineering. Biomaterials 2000;21:2347–59. [PubMed: 11055282]
5. Rezwan K, Chen QZ, Blaker JJ, Boccaccini AR. Biodegradable and bioactive porous polymer/inorganic composite scaffolds for bone tissue engineering. Biomaterials 2006;27:3413–31. [PubMed: 16504284]
6. Clarke KI, Graves SE, Wong ATC, Triffitt JT, Francis MJO, Czernuszka JT. Investigation into the formation and mechanical-properties of a bioactive material based on collagen and calcium phosphate. J Mater Sci -Mater Med 1993;4:107–10.
7. Tenhuisen KS, Martin RI, Klimkiewicz M, Brown PW. Formation and properties of a synthetic bone composite: hydroxyapatite-collagen. J Biomed Mater Res 1995;29:803–10. [PubMed: 7593018]
8. Du C, Cui FZ, Feng QL, Zhu XD, de Groot K. Tissue response to nano-hydroxyapatite/collagen composite implants in marrow cavity. J Biomed Mater Res 1998;42:540–8. [PubMed: 9827677]
9. Tenhuisen KS, Brown PW. The formation of hydroxyapatite-gelatin composites at 38 degrees C. J Biomed Mater Res 1994;28:27–33. [PubMed: 8126026]
10. Kim HW, Kim HE, Salih V. Stimulation of osteoblast responses to biomimetic nanocomposites of gelatin-hydroxyapatite for tissue engineering scaffolds. Biomaterials 2005;26:5221–30. [PubMed: 15792549]
11. Thomson RC, Yaszemski MJ, Powers JM, Mikos AG. Hydroxyapatite fiber reinforced poly(α-hydroxy ester) foams for bone regeneration. Biomaterials 1998;19:1935–43. [PubMed: 9863527]
12. Zhang R, Ma PX. Poly(α-hydroxyl acids)/hydroxyapatite porous composites for bone-tissue engineering. I. Preparation and morphology. J Biomed Mater Res 1999;44:446–55. [PubMed: 10397949]
13. Rizzi SC, Heath DJ, Coombes AGA, Bock N, Textor M, Downes S. Biodegradable polymer/hydroxyapatite composites: surface analysis and initial attachment of human osteoblasts. J Biomed Mater Res 2001;55:475–86. [PubMed: 11288075]
14. Wei G, Ma PX. Structure and properties of nano-hydroxyapatite/polymer composite scaffolds for bone tissue engineering. Biomaterials 2004;25:4749–57. [PubMed: 15120521]
15. Kim SS, Ahn KM, Park MS, Lee JH, Choi CY, Kim BS. A poly(lactide-*co*-glycolide)/hydroxyapatite composite scaffold with enhanced osteoconductivity. J Biomed Mater Res A 2007;80:206–15. [PubMed: 17072849]
16. Causa F, Netti PA, Ambrosio L, Ciapetti G, Baldini N, Pagani S, Martini D, Giunti A. Poly-ε-caprolactone/hydroxyapatite composites for bone regeneration: in vitro characterization and human osteoblast response. J Biomed Mater Res A 2006;76:151–62. [PubMed: 16258959]
17. Wiria FE, Leong KF, Chua CK, Liu Y. Poly-ε-caprolactone/hydroxyapatite for tissue engineering scaffold fabrication via selective laser sintering. Acta Biomater 2007;3:1–12. [PubMed: 17055789]
18. Jie W, Yubao L. Tissue engineering scaffold material of nano-apatite crystals and polyamide composite. Eur Polym J 2004;40:509–15.
19. Moursi AM, Winnard AV, Winnard PL, Lannutti JJ, Seghi RR. Enhanced osteoblast response to a polymethylmethacrylate-hydroxyapatite composite. Biomaterials 2002;23:133–44. [PubMed: 11762831]

20. Zhang R, Ma PX. Porous poly(L-lactic acid)/apatite composites created by biomimetic process. J Biomed Mater Res 1999;45:285–93. [PubMed: 10321700]
21. Chou YF, Dunn JC, Wu BM. In vitro response of MC3T3-E1 preosteoblasts within three-dimensional apatite-coated PLGA scaffolds. J Biomed Mater Res B Appl Biomater 2005;75:81–90. [PubMed: 16001421]
22. Hong Z, Qiu X, Sun J, Deng M, Chen X, Jing X. Grafting polymerization of L-lactide on the surface of hydroxyapatite nano-crystals. Polymer 2004;45:6699–706.
23. Qiu X, Hong Z, Hu J, Chen L, Chen X, Jing X. Hydroxyapatite surface modified by L-lactic acid and its subsequent grafting polymerization of L-lactide. Biomacromolecules 2005;6:1193–9. [PubMed: 15877333]
24. Hong Z, Zhang P, He C, Qiu X, Liu A, Chen L, Chen X, Jing X. Nano-composite of poly(L-lactide) and surface grafted hydroxyapatite: mechanical properties and biocompatibility. Biomaterials 2005;26:6296–304. [PubMed: 15913758]
25. Liao SS, Cui FZ, Zhang W, Feng QL. Hierarchically biomimetic bone scaffold materials: nano-HA/collagen/PLA composite. J Biomed Mater Res B Appl Biomater 2004;69:158–65. [PubMed: 15116405]
26. Peter SJ, Miller MJ, Yasko AW, Yaszemski MJ, Mikos AG. Polymer concepts in tissue engineering. J Biomed Mater Res 1998;43:422–7. [PubMed: 9855200]
27. Wang S, Lu L, Yaszemski MJ. Bone-tissue-engineering material poly(propylene fumarate): correlation between molecular weight, chain dimensions, and physical properties. Biomacromolecules 2006;7:1976–82. [PubMed: 16768422]
28. He S, Timmer MD, Yaszemski MJ, Yasko AW, Engel PS, Mikos AG. Synthesis of biodegradable poly(propylene fumarate) networks with poly(propylene fumarate)-diacylate macromers as crosslinking agents and characterization of their degradation products. Polymer 2001;42:1251–60.
29. Yaszemski MJ, Payne RG, Hayes WC, Langer RS, Aufdemorte TB, Mikos AG. The ingrowth of new bone tissue and initial mechanical properties of a degrading polymeric composite scaffold. Tissue Eng 1995;1:41–52.
30. Peter, SJ.; Miller, MJ.; Yaszemski, MJ.; Mikos, AG. 5. Poly(propylene fumarate). In: Domb, AJ.; Kost, J.; Wiseman, DM., editors. Handbook of biodegradable polymers. Amsterdam: Harwood Academic Publishers; 1997. p. 87-97.
31. Kharas GB, Kamenetsky M, Simantirakis J, Beinnlich KC, Rizzo AMT, Caywood GA, Watson K. Synthesis and characterization of fumarate-based polyesters for use in bioresorbable bone cement composites. J Appl Polym Sci 1997;66:1123–37.
32. Wang S, Lu L, Gruetzmacher JA, Currier BL, Yaszemski MJ. A biodegradable and crosslinkable multiblock copolymer consisting of poly(propylene fumarate) and poly(ε-caprolactone): synthesis, characterization, and physical properties. Macromolecules 2005;38:7358–70.
33. Peter SJ, Kim P, Yasko AW, Yaszemski MJ, Mikos AG. Crosslinking characteristics of an injectable poly(propylene fumarate)/ β-tricalcium phosphate paste and mechanical properties of the crosslinked composite for use as a biodegradable bone cement. J Biomed Mater Res 1999;44:314–21. [PubMed: 10397934]
34. Peter SJ, Lu L, Kim DJ, Mikos AG. Marrow stromal osteoblast function on a poly(propylene fumarate)/β-tricalcium phosphate biodegradable orthopaedic composite. Biomaterials 2000;21:1207–13. [PubMed: 10811302]
35. Jayabalan M, Thomas V, Sreelatha PK. Studies on poly(propylene fumarate-co-ethylene glycol) based bone cement. Biomed Mater Eng 2000;10:57–71. [PubMed: 11086840]
36. Hakimimehr D, Liu DM, Troczynski T. In-situ preparation of poly(propylene fumarate)—hydroxyapatite composite. Biomaterials 2005;26:7297–303. [PubMed: 16026822]
37. Lee KW, Wang S, Lu L, Jabbari E, Currier BL, Yaszemski MJ. Fabrication and characterization of poly(propylene fumarate) scaffolds with controlled pore structures using 3-dimensional printing and injection molding. Tissue Eng 2006;12:2801–11. [PubMed: 17518649]
38. Rumpler M, Woesz A, Varga F, Manjubala I, Klaushofer K, Fratzl P. Three-dimensional growth behavior of osteoblasts on biomimetic hydroxyapatite scaffolds. J Biomed Mater Res A 2007;81:40–50. [PubMed: 17109410]

39. Chang MC, Ko CC, Douglas WH. Preparation of hydroxyapatite-gelatin nanocomposite. Biomaterials 2003;24:2853–62. [PubMed: 12742723]
40. Murugan R, Ramakrishna S. Development of nanocomposites for bone grafting. Compos Sci Technol 2005;65:2385–2406.
41. Vandiver J, Dean D, Patel N, Bonfield W, Ortiz C. Nanoscale variation in surface charge of synthetic hydroxyapatite detected by chemically and spatially specific high-resolution force spectroscopy. Biomaterials 2005;26:271–83. [PubMed: 15262469]
42. Elgendy HM, Norman ME, Keaton AR, Laurencin CT. Osteoblast-like cell (MC3T3-E1) proliferation on bioerodible polymers: an approach towards the development of a bone-bioerodible polymer composite material. Biomaterials 1993;14:263–9. [PubMed: 8386557]
43. Anselme K. Osteoblast adhesion on biomaterials. Biomaterials 2000;21:667–81. [PubMed: 10711964]
44. Harbers, GM.; Grainger, DW. 3. Cell-material interactions: Fundamental design issues for tissue engineering and clinical considerations. In: Guelcher, SA.; Hollinger, JO., editors. An Introduction to Biomaterials. Boca Raton: CRC Press Taylor & Francis Group; 2006. p. 20-24.
45. Iuliano DJ, Saavedra SS, Truskey GA. Effect on the conformation and orientation of adsorbed fibronectin on endothelial cell spreading and the strength on adhesion. J Biomed Mater Res 1993;27:1103–13. [PubMed: 8408123]
46. Ruardy TG, Schakenraad JM, van der Mei HC, Busscher HJ. Adhesion and spreading of human skin fibroblasts on physicochemically characterized gradient surfaces. J Biomed Mater Res 1995;29:1415–23. [PubMed: 8582910]
47. Hayman EG, Pierschbacher MD, Suzuki S, Ruoslahti E. Vitronectin—a major cell attachment-promoting protein in fetal bovine serum. Exp Cell Res 1985;160:245–58. [PubMed: 2412864]
48. Grinnell F. Focal adhesion sites and the removal of substratum-bound fibronectin. J Cell Biol 1986;103:2697–706. [PubMed: 2947902]
49. Woo KM, Seo J, Zhang R, Ma PX. Suppression of apoptosis by enhanced protein adsorption on polymer/hydroxyapatite composite scaffolds. Biomaterials 2007;28:2622–30. [PubMed: 17320948]
50. Kennedy SB, Washburn NR, Simon CG Jr, Amis EJ. Combinational screen of the effect of surface energy on fibronectin-mediated osteoblast adhesion, spreading, and proliferation. Biomaterials 2006;27:3817–24. [PubMed: 16563495]

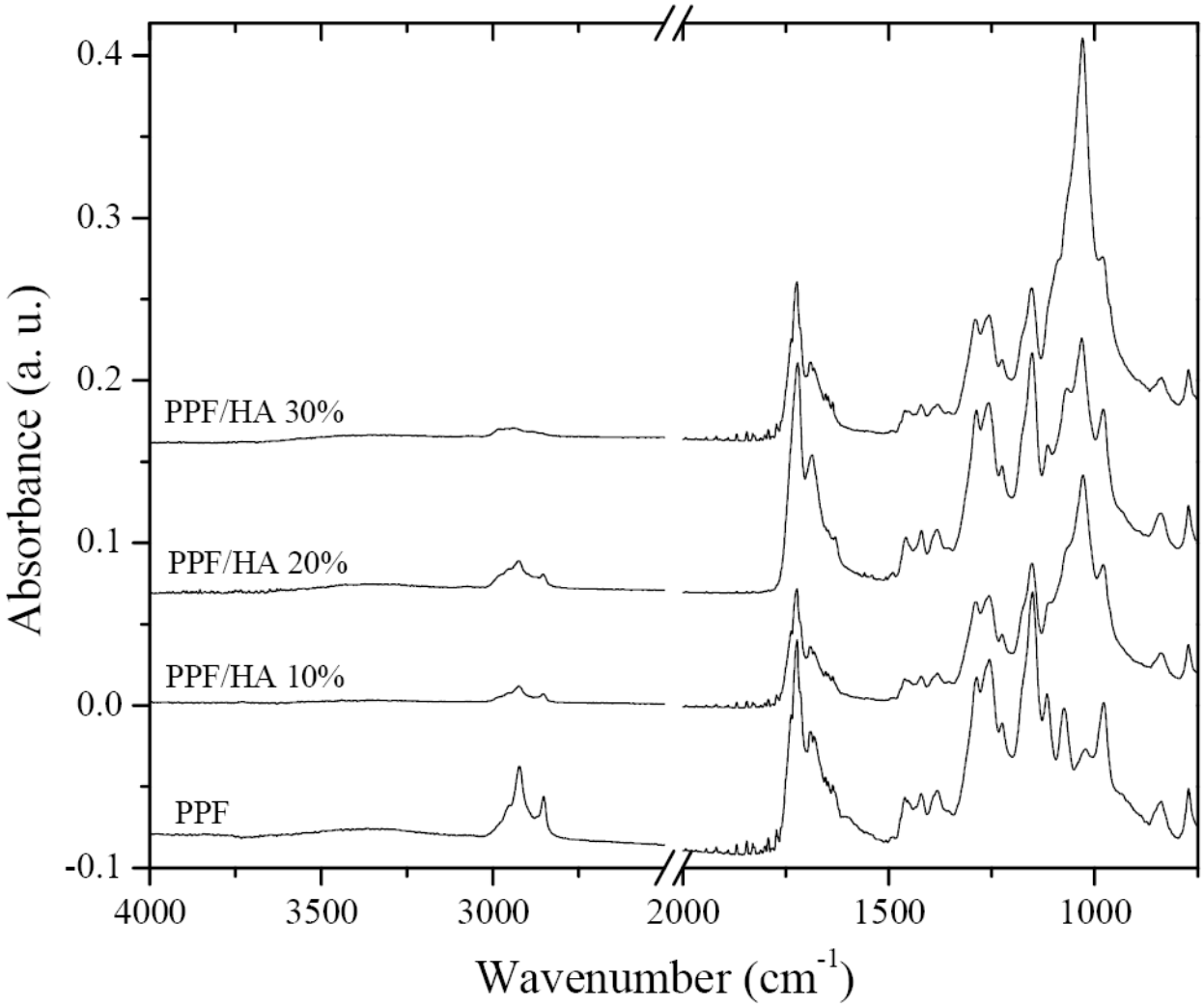

Figure 1.
FTIR spectra of crosslinked PPF and PPF/HA with different HA contents.

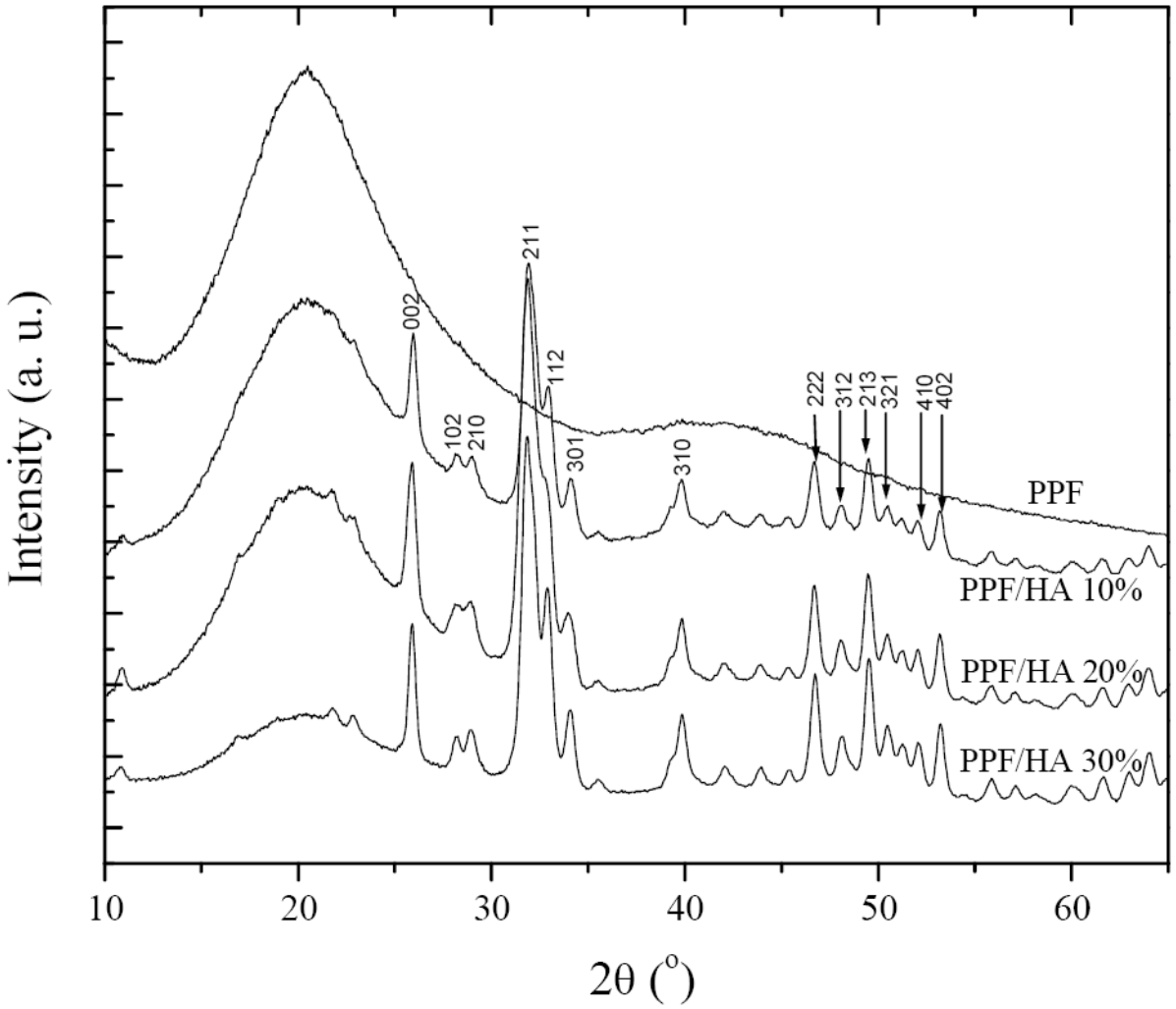

Figure 2.
Wide-angle X-ray diffraction patterns of crosslinked PPF and PPF/HA with different HA contents. HA peaks were indexed according to the JCPDS 9-432 standard.

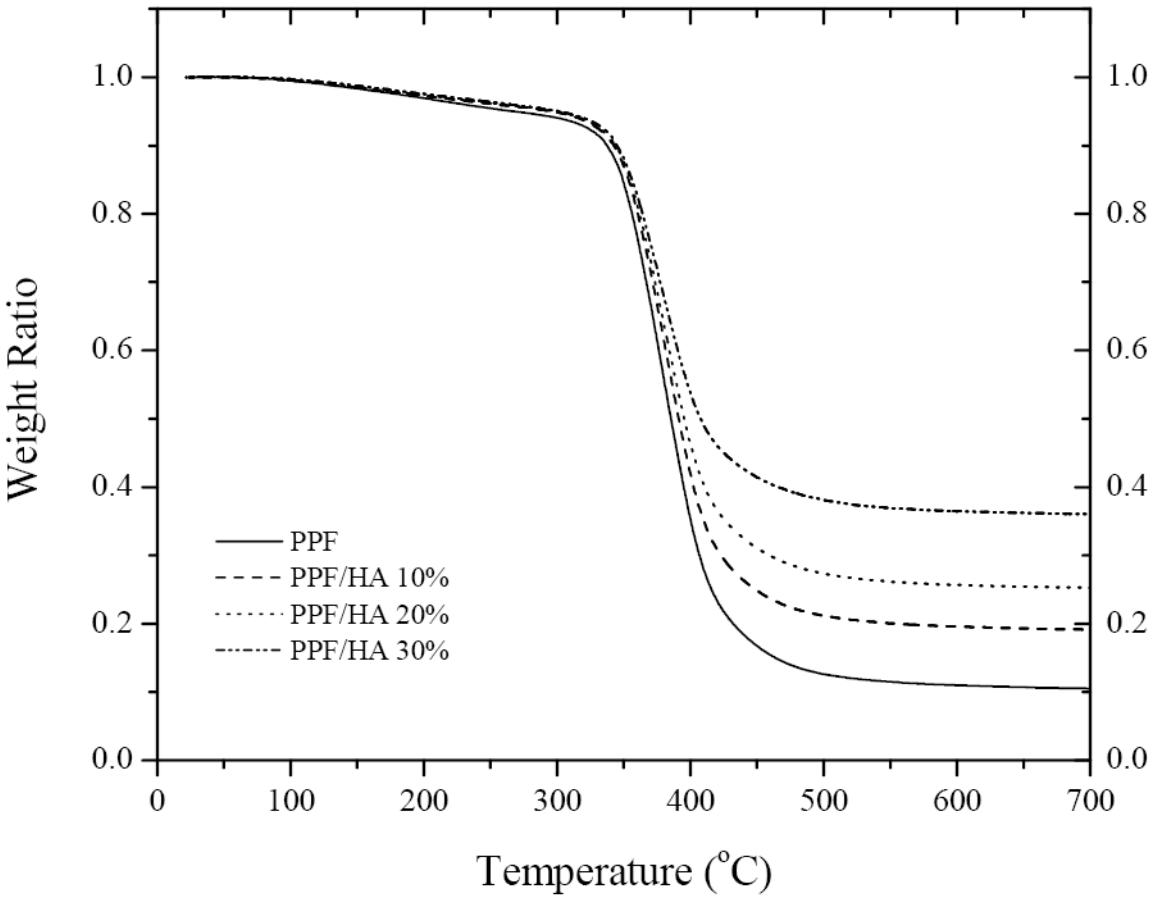

Figure 3.
TGA thermograms of crosslinked PPF and PPF/HA with different HA contents.

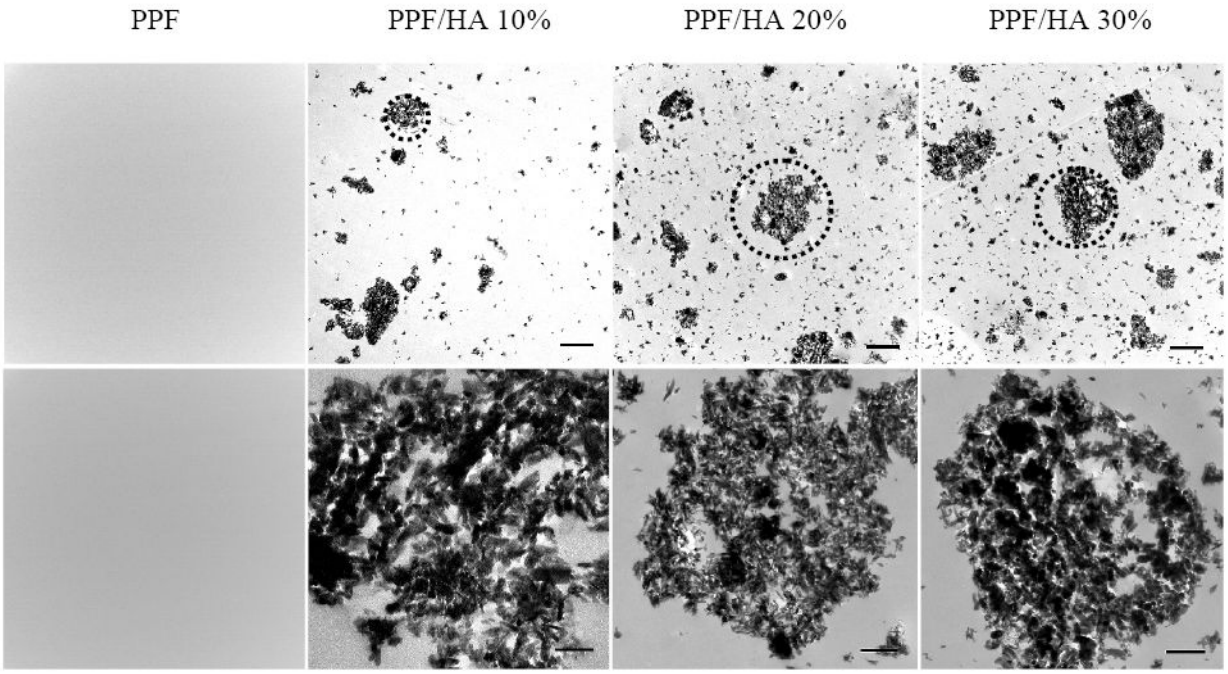

Figure 4.
Transmission electron micrographs of crosslinked PPF and PPF/HA disks with different HA contents. Bottom images were magnified from the dotted areas of the top images. Scale bars represent 2 μm (top) and 500 nm (bottom).

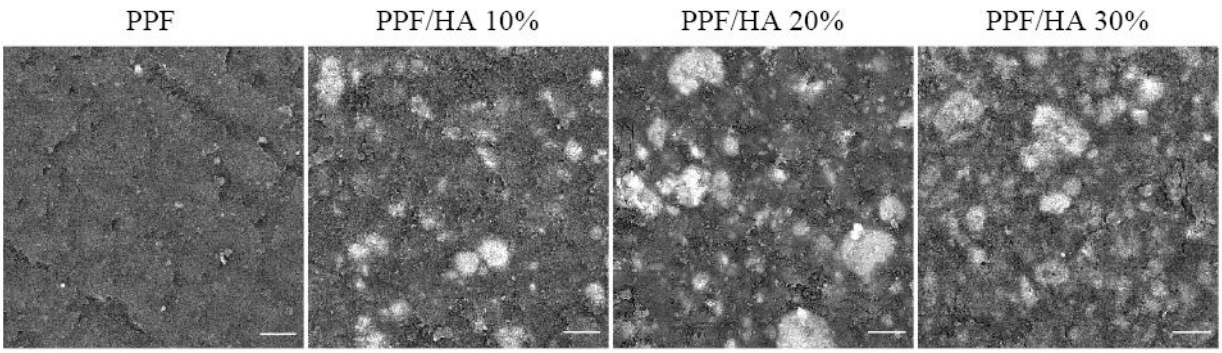

Figure 5.
Scanning electron micrographs of crosslinked PPF and PPF/HA disks with different HA contents. White spots in each image show the location of HA nanoparticles. Scale bars represent 10 μm.

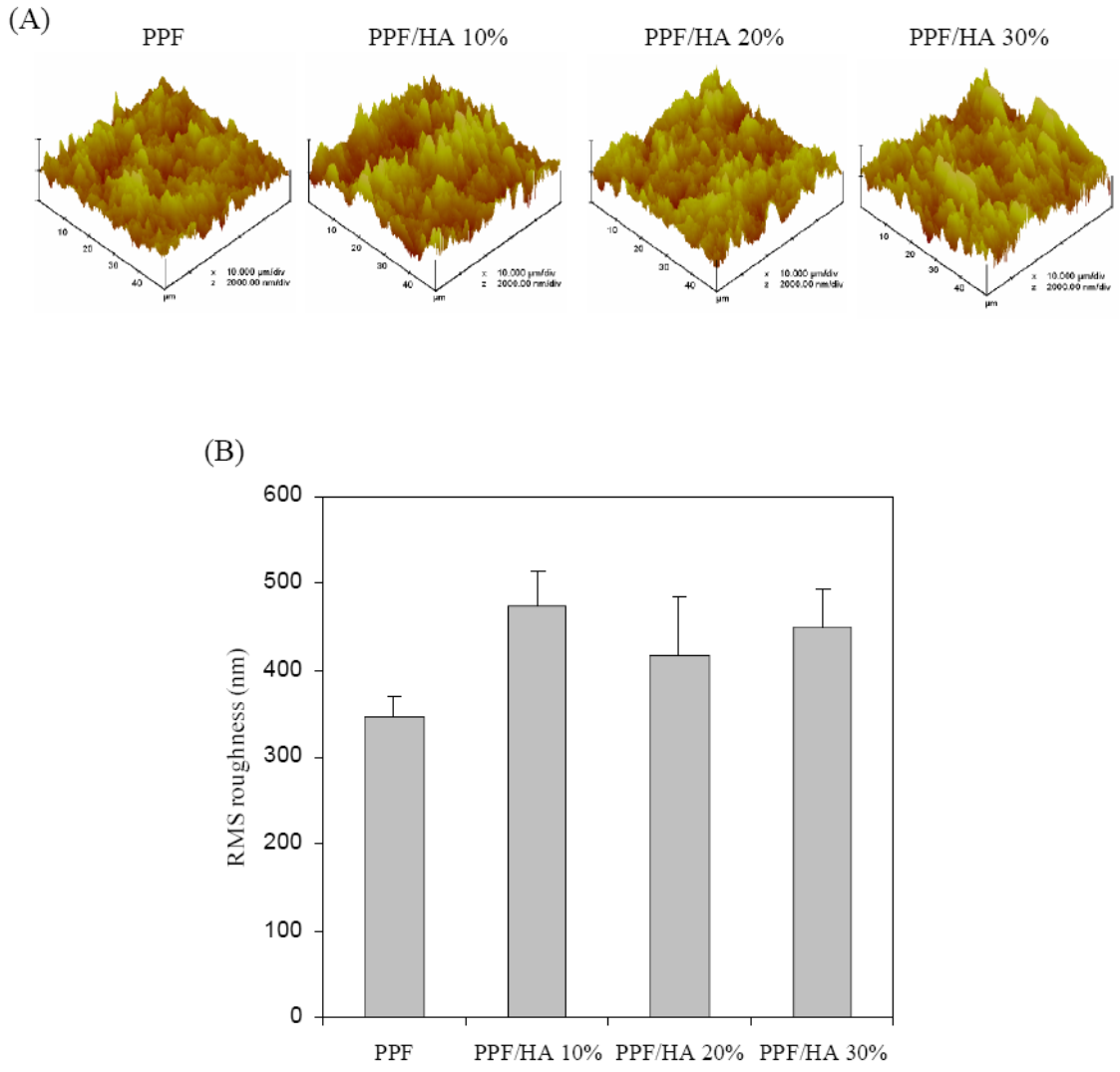

Figure 6.

Atomic force micrographs of crosslinked PPF and PPF/HA disks with different HA contents. (a) 3D scan images (scan size = 50 μm, scan rate = 3.924 Hz, number of samples = 512, and data scale = 2.0 μm). (b) Root mean square (RMS) roughness of the samples. No statistical difference was detected among the sample groups (p>0.05).

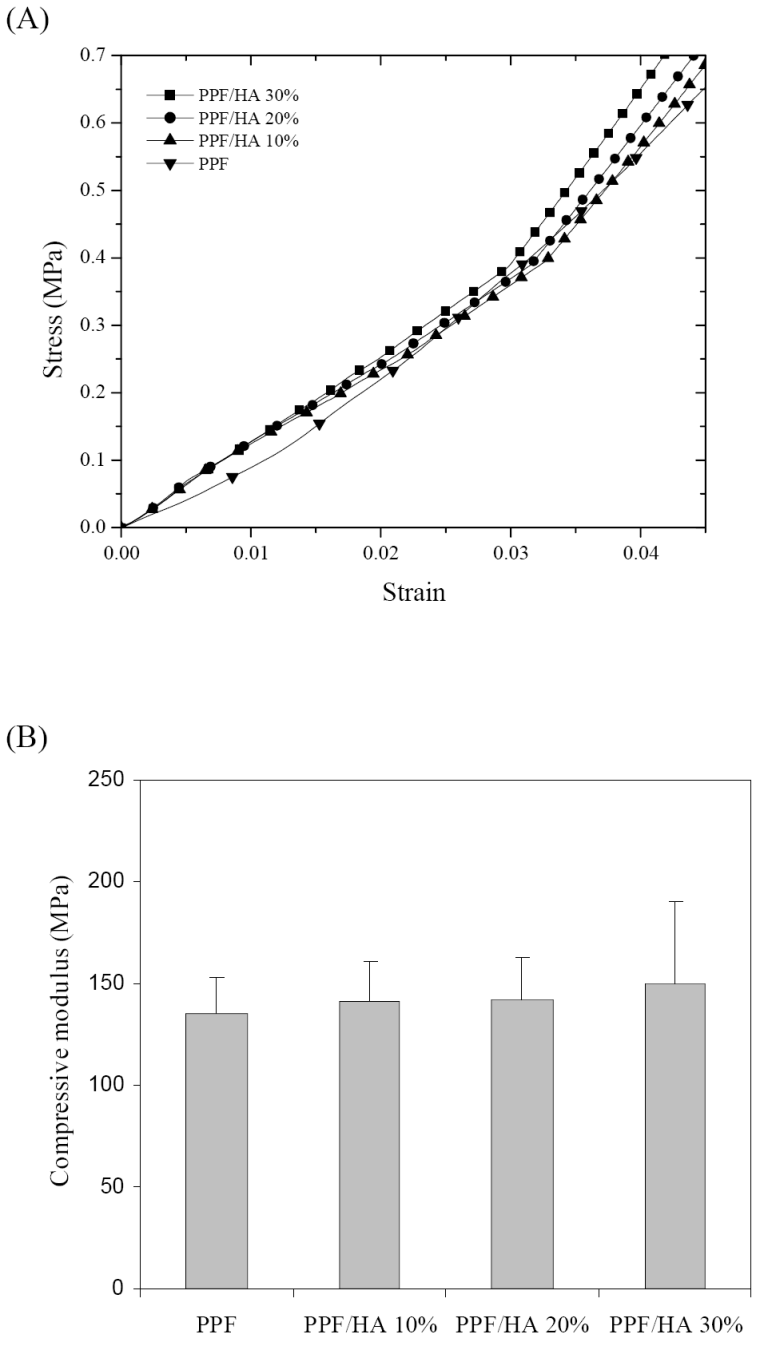

Figure 7.
(a) Compressive stress-strain curves and (b) compressive moduli of crosslinked PPF and PPF/HA disks with different HA contents.

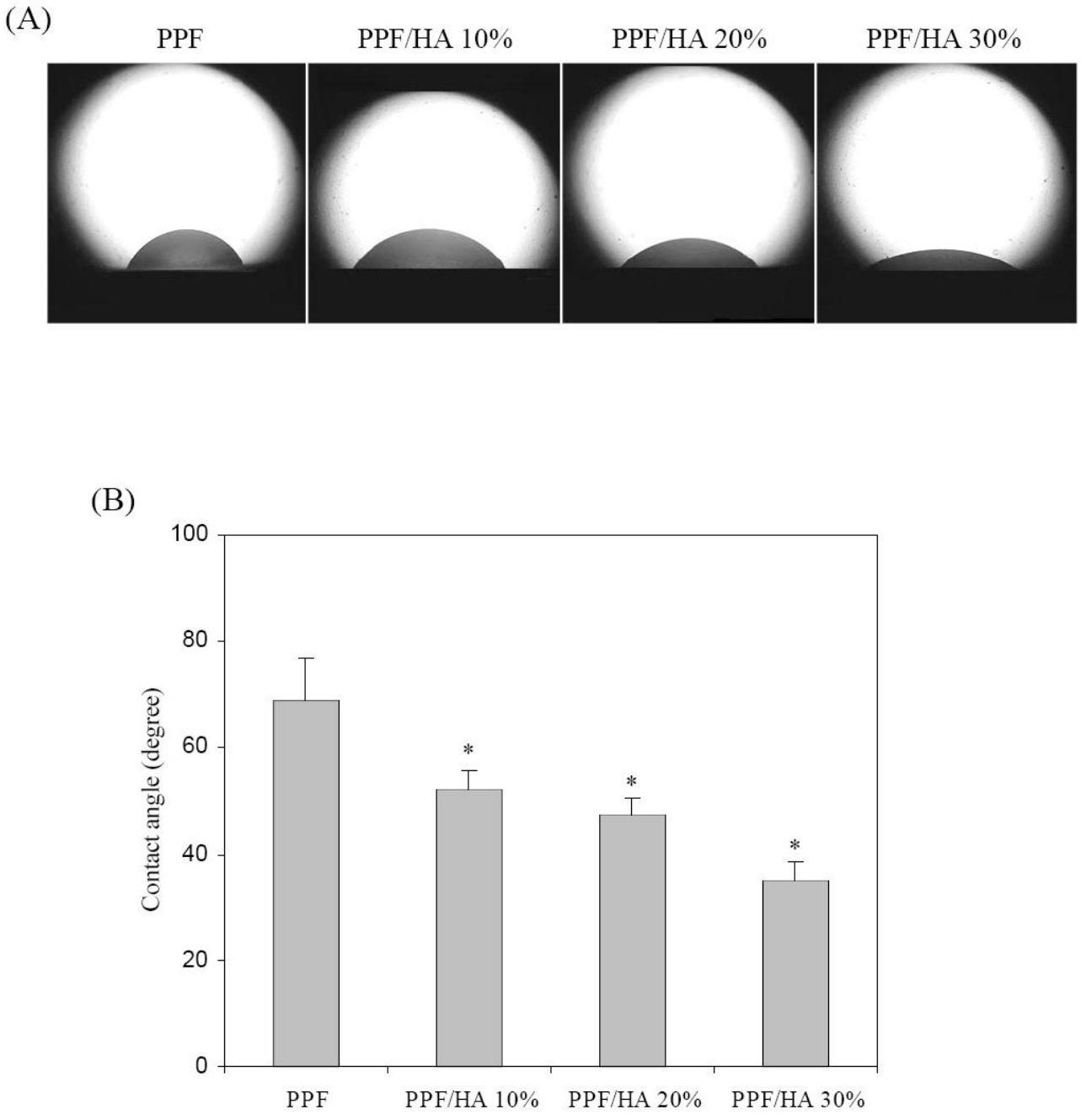

Figure 8.

(a) Photographs of water droplets on the surface of crosslinked PPF and PPF/HA disks with different HA contents. (b) Water contact angles calculated from the tangent method. * $p<0.05$ compared to data on crosslinked PPF.

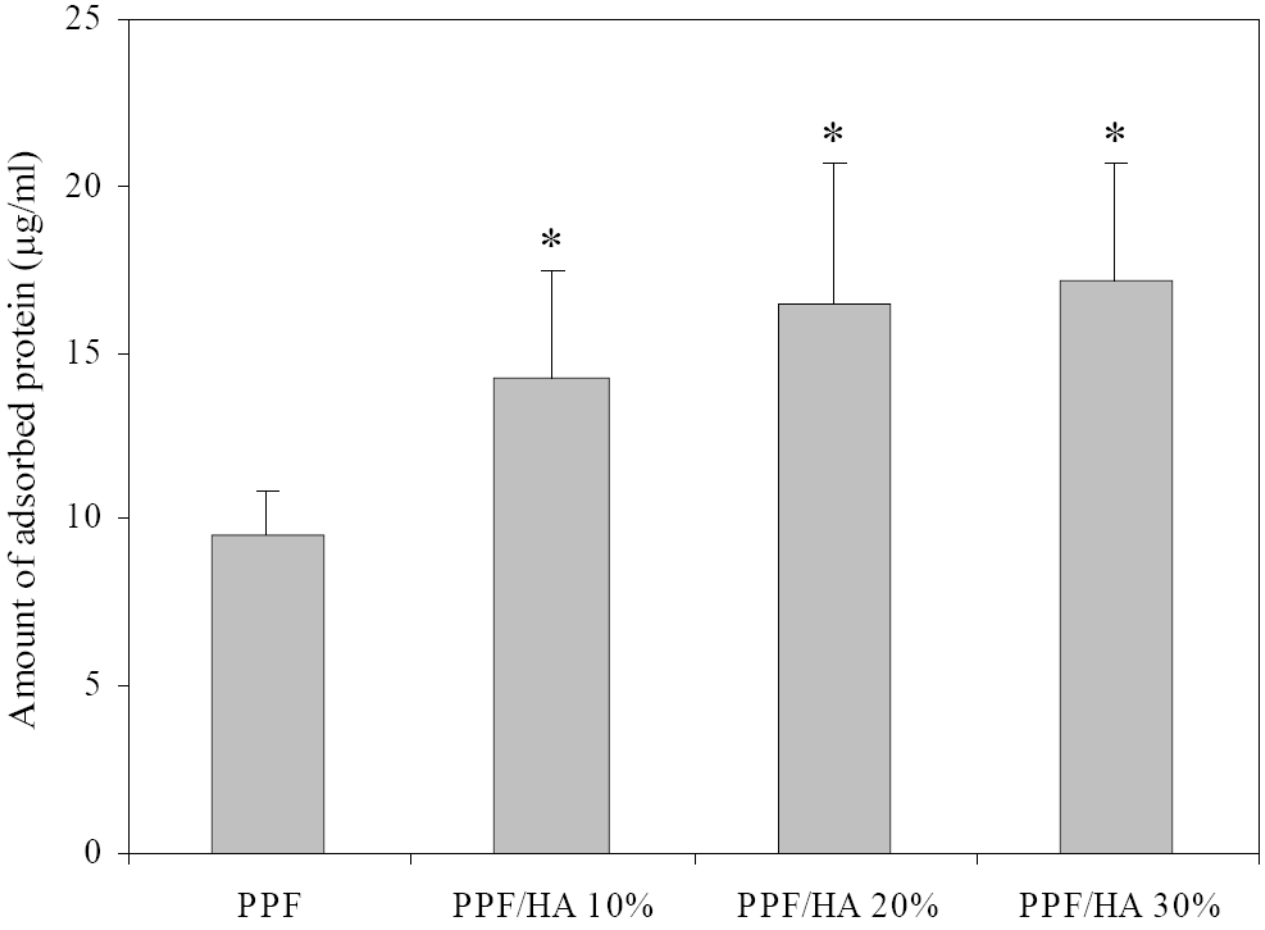

Figure 9.
Amount of adsorbed proteins on crosslinked PPF and PPF/HA disks with different HA contents. * $p<0.05$ compared to data on crosslinked PPF.

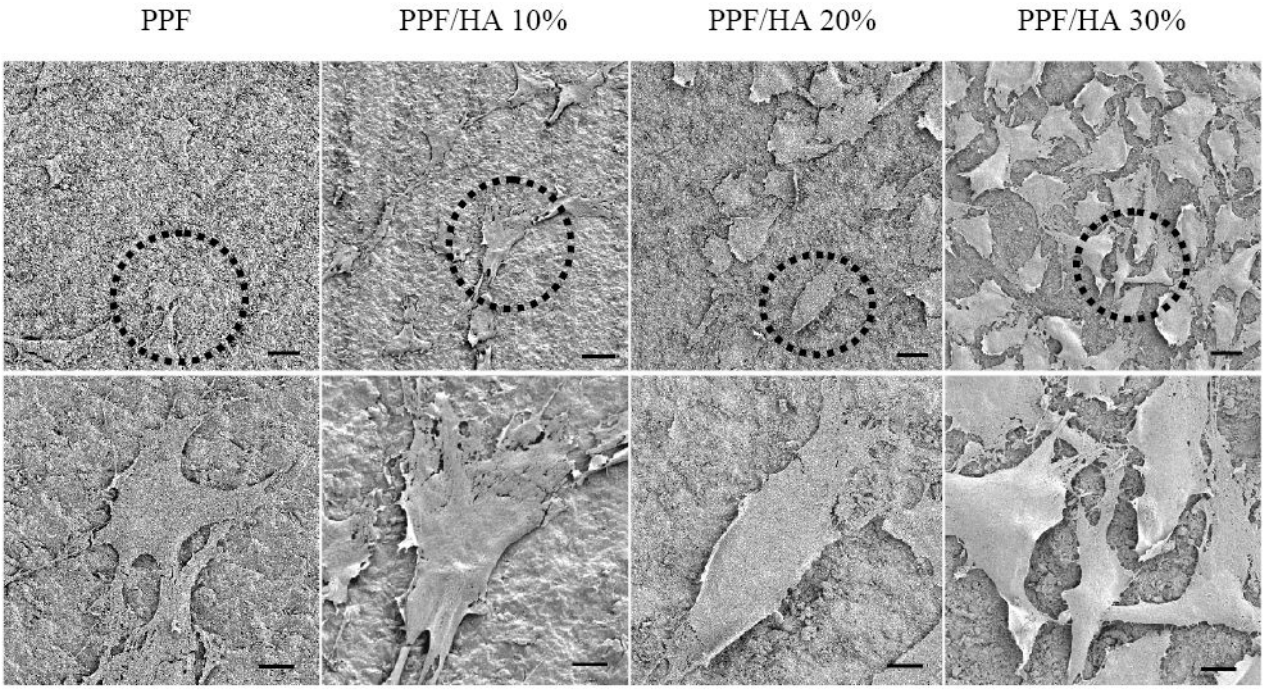

Figure 10.
Scanning electron micrographs of MC3T3 cells after 24 h seeding on crosslinked PPF and PPF/HA disks with different HA contents. Bottom images were magnified from the dotted areas of the top images. Scale bars represent 300 μm (top) and 10 μm (bottom).

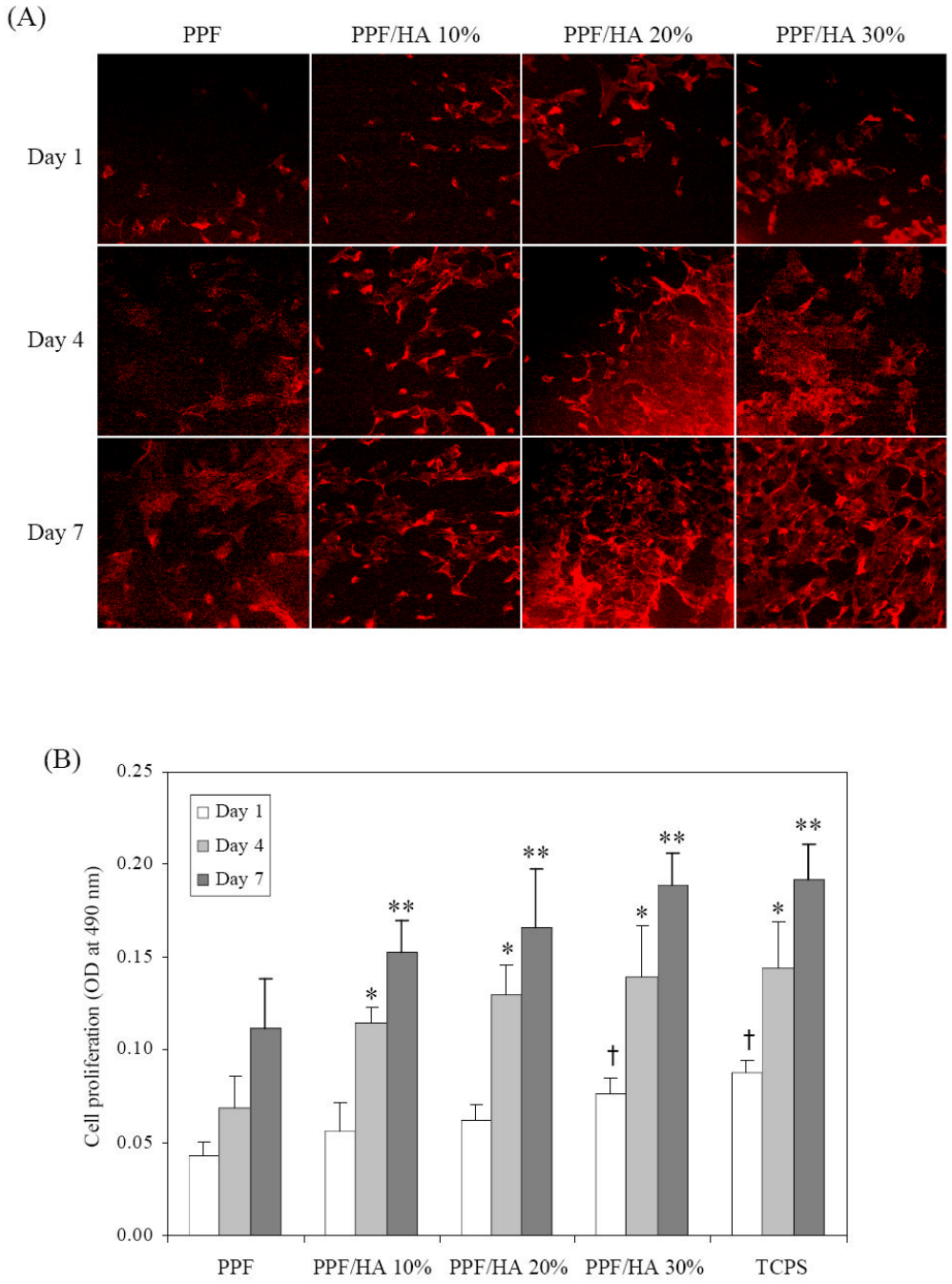

Figure 11.
F-actin staining with rhodamin-phalloidin of MC3T3 cells after 1, 4, and 7 days of culture on crosslinked PPF and PPF/HA disks with different HA contents.

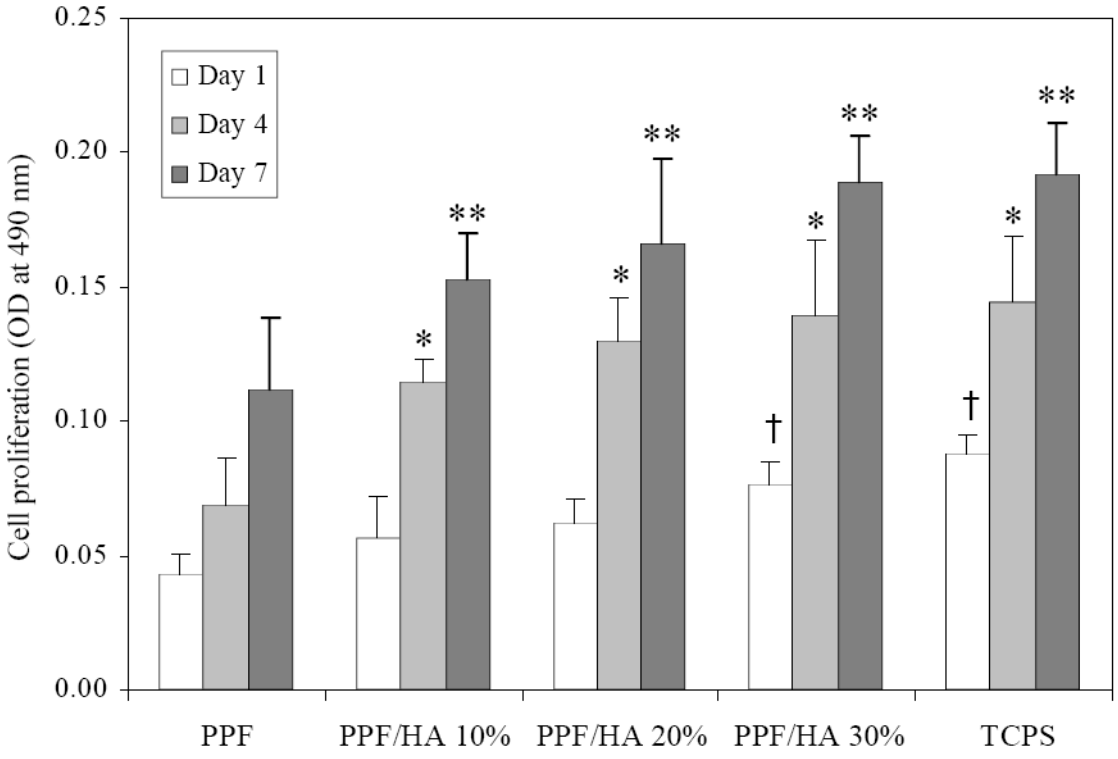

Figure 12.
MC3T3 cell proliferation on crosslinked PPF and PPF/HA disks, as assessed by MTS absorption at 490 nm. Tissue culture polystyrene (TCPS) serves as a positive control. *, **, † $p<0.05$ compared to data on crosslinked PPF at each time point.

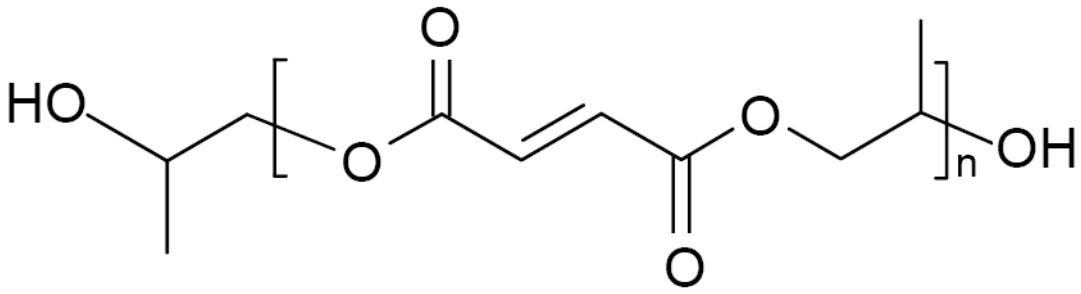

Scheme 1.
Chemical structure of PPF.

Table 1

Compositions of PPF/HA mixtures for nanocomposite fabrication via chemical crosslinking.

PPF (g)	NVP (g)	Nano-HA (g) (wt.%)	BPO (μl)	DMT (μl)
1	0.4	0 (0) 0.156 (10) 0.350 (20) 0.600 (30)	40	16